

000
001
002
003
004
005
006
007
008
009
010
011054
055
056
057
058
059
060
061
062
063
064
065
066
067
068
069
070
071
072
073
074
075
076
077
078
079
080
081
082
083
084
085
086
087
088
089
090
091
092
093
094
095
096
097
098
099
100
101
102
103
104
105
106
107

Deformable Diversity Similarity for Partial Matching of 3D Shapes

Anonymous CVPR submission

Paper ID ****

Abstract

We propose a novel approach for the matching of partial deformable shapes in 3D. Inspired by recent advances in 2D template matching techniques, our method relies on the concept of deformable diversity similarity(DDIS), extends and adapts it from an image to the 3D shape domain, and leverages the distinct behavior of this framework in different scales to achieve shape correspondences. We evaluate this framework on the SHREC16 partial matching of deformable shapes and show state of the art performance in achieving sparse correspondences.

1. Introduction

Shape correspondence is a fundamental and challenging problem in computer vision and graphics. It has usage in various applications such as transferring texture and animation. Shapes rarely, if ever manifest in only one pose. While rigid transformations between surfaces is a well researched topic with many adequate solutions, a more challenging problem arises when a shape is deformed non-rigidly, a case all too common for people, animals and objects. Moreover, the shape acquisition process almost always lead to partiality of the scanned object. Occlusions arise from different angles of acquisition, which cause an object to occlude itself, or stem from other occluding objects. An additional type of difficulty which might be occur is topological noise, occurring when shapes touch pn another, thus making sensors unable to seperate them. All of these combined give rise to the challenging problem of partial correspondences, where a deformed and incomplete shape, possibly with topological changes, has to be matched with its full version. The goal of this paper is to deal with this challenging problem.

While in a rigid setting the problem can be solved by RANSAC and ICP like approaches[20, 10], extending these to non-rigid case produces mediocre results due to an underlying assumption of small deformations. Early methods specialized for the non-rigid problem focused on minimization of intrinsic metric distortion[6, 27, ?] and regularity of

parts[?, 4]. These methods all contain with them a global assumption of isometry which holds only approximately, these tended to break down with it, and are also unable to handle extreme partiality. Another family of method is based on functional correspondence. These methods model correspondences as a linear operator of a known nature between a space of functions on manifolds[15]. These methods, originally designed for the full shape correspondence scenario have achieved state of the art results on various partial matching tasks in the recent years[13, 28, 18], and produce dense correspondence maps, but are not parallelizable, and their reliance on intrinsic metrics makes them invariant to symmetry.

We take a different approach. We take advantage of the fact that while the isometric property tends to break over large distances, it usually holds approximately in limited environments. These also tend to suffer a lot less from boundary effects, especially when concentrated around the extremities of a shape.

We can thus treat the problem of partial correspondences as matching of multiple templates, each smaller then the partial surface centered around shape landmarks.

In addition, since point descriptors are known to be modified by partiality and deformations, instead of using them directly, we follow the approach off[26](DDIS) which tackles template matching in 2D and use simple statistical assumptions on the nature of nearest neighbors between small patch descriptors, along with the assumption of small deformations in medium environments to obtain similarity scores between these partial shape templates.

We analyze the behavior of DDIS similarity in different scales and devise a multi scale scheme which leverages the advantages of each scale while masking their shortcomings.

We show that using this approach, we are able to generate a set of sparse correspondences, which are less prone to symmetrical assignment than functional correspondence reliant methods, and are of superior quality on the SHREC16 Partial matching challenge[8]. We then demonstrate how these sparse correspondences can be used as an input to existing functional correspondence algorithms to obtain dense correspondences or a higher quality.

108 In summary, our contributions are:
 109

- 110 • A non trivial extension of Deformable Diversity from
 111 2 to 3 Dimensions.
- 112
- 113 • A modified DDIS similarity measure which is more
 114 well suited to handle matching of templates with a dif-
 115 ferent number of points.
- 116
- 117 • An empirical analysis of DDIS behavior in different
 118 scales, leading to an improved multi-scale framework.
- 119
- 120 • A novel multi-template approach to partial matching
 121 of deformable shapes which can both produce state of
 122 the art sparse correspondences, and be used as an input
 123 to functional correspondence algorithms, significantly
 124 improving the results obtained by these.
- 125

126 The rest of the work is organized as follows: in section
 127 2 we go over related works in the field of shape analysis.
 128 Section 3 introduces our Deformable Diversity framework
 129 for 3D shape matching. Experiments and results are given
 130 in section 4, and the conclusions are in section 5. **2. What
 131 previous work suggested -key ideas and drawbacks**

- 132 3. Our key ideas
- 133 4. Our results
- 134 5. Major contributions
- 135 6. Roadmap

137 2. Related work

138 2.1. Matching Of Surfaces

139 As a fundamental problem in computer graphics and vi-
 140 sion, an extensive body of work have been done on the
 141 matching of surfaces. For the rigid setup an adequate solu-
 142 tion exists. Iterative Closest Point(ICP)[1] algorithm, pre-
 143 ceded by initial alignment[22] tackle partial matching suc-
 144 cessfully. Adapting this to the rigid setup however has
 145 proved to have limited success due to the alignment which
 146 is necessary, and thus is only fit for very small non-rigid
 147 deformation. In contrast, early non-rigid correspondence
 148 methods were designed to work in the scenarios of little to
 149 no partiality. The assumption of near isometry[6] has been
 150 used commonly. This assumption is usually broken in the
 151 partial setup. Recent works, which address the full corre-
 152 spondence problem[2, 14, 25, 29] manage to cope with dis-
 153 tortion by using smarter optimization objectives, but use the
 154 assumption of a bijection between the shapes, and thus can-
 155 not handle significant partiality.

156 2.2. Partial Matching of Deformable shapes

157 Early works which were designed with partial match-
 158 ing in mind[4, 5] solved a combined optimization problem

159 over the metric distortion and the regularity of correspond-
 160 ing parts. Following works relaxed the regularity require-
 161 ment by allowing for sparse correspondence[27] and con-
 162 trolling the sparsity of which [19]. Other metric distortion
 163 based works[23, 24] minimized the distortion metric over
 164 the shape extremities by doing combinatorial search of least
 165 distortion matches and then densify while refining them in
 166 the process. In addition to only supplying sparse correspon-
 167 dences and having a high computational complexity, relying
 168 only on the intrinsic distortion metric makes these methods
 169 fail when boundary effects plays a significant role.

170 In[16] a bag of words point-wise descriptors on a part in
 171 conjunction with a constraint on area similarity and the reg-
 172 ularity of the boundary length to produce correspondence
 173 less matching parts without point to point correspondences.

174 Another notable family of works are derived from func-
 175 tional correspondences. Introduced at[15] these assume that
 176 correspondences between spaces of functions on a manifold
 177 can be modeled as a linear operators, approximately diagno-
 178 nal given a smart choice of functions, which, given a small
 179 set of known correspondences can be recovered. The orig-
 180 inal paper used the Laplace Beltrami eigenfunctions. Fol-
 181 lowing works employed joint diagnozilization of the Lapla-
 182 cian matrices to find an optimal basis, and[17] extended it
 183 to the setting where the order of the functions is unknown,
 184 by solving for permutation of correspondence as well. It
 185 has been shown in [12] that matrix completion can address
 186 non-isometry and mild partiality. A combination with heat
 187 kernels as a distortion metric[28] has been shown to be
 188 able to handle some partiality, given an initialization with
 189 sparse correspondences, but this relies heavily on obtaining
 190 good initial correspondences, and thus application to partial
 191 matching has only been shown as a proof of concept.

192 Recently [18] had proven that partiality induces a slanted
 193 diagonal structure in the correspondence matrix and found
 194 the Laplacian eigenfunctions from each basis which induces
 195 this structure. Current state of the art[13] uses this notion
 196 in conjunction with joint diagnozilization. The main draw-
 197 back of this method, shared with other intrinsic methods, is
 198 its invariance to symmetries. In addition, using sequential
 199 optimization, the entire family of methods cannot be paral-
 200 lelized.

201 **3D Shape Descriptors** A fundamental building block in
 202 many shape analysis tasks are shape descriptors , these are
 203 mappings $f_{\mathcal{M}} : \mathcal{M} \rightarrow \mathbb{R}^q, f_{\mathcal{N}} : \mathcal{N} \rightarrow \mathbb{R}^q$ which are con-
 204 structed in a way which embeds similar shapes close in a
 205 euclidean space of dimension q . Shape descriptors of the
 206 extrinsic variety such as PFH[21], SHOT and FPFH[20]
 207 which are usually calculated in euclidean space and are thus
 208 sensitive to non rigid deformations, but are generally bet-
 209 ter in discerning between symmetrical shapes, and are also
 210 more robust to noise, topology artifacts and boundaries. On
 211 the other hand intrinsic features such as Heat[7] and Wave

216 Kernel signatures[3] are invariant under isometric transformations,
 217 but are very sensitive to partiality and are unable
 218 to discern between symmetric parts.
 219

220 2.3. Template matching in 2D

221 Template matching in 2D is a well researched topic.
 222 Similarly to 3D objects are going complex deformations of
 223 pose, and are only seen partially depending on the camera
 224 point of view. Recently a series of works which use a very
 225 simplistic framework based on the statistical properties of
 226 nearest neighbors in low level feature space had made good
 227 strides in tackling this complex task.
 228

229 **Best Buddies Similarity** Great strides had been
 230 achieved in the field of 2D template matching. Best Buddies
 231 Similarity[9] is a simple framework which employs a statis-
 232 tical assumption in which between two windows containing
 233 the same template \mathcal{N}, \mathcal{M} patches maintain Bi Directional
 234 Similarity. That is - given a point $n_i \in \mathcal{N}$ and a correspond-
 235 ing point $m_i \in \mathcal{M}$ they should maintain a relationship of
 236 Bi-Directional Similarity - that is if $NN_{\mathcal{M}}(n_i) = m_j$ then
 237 on a matching template we should expect $NN_{\mathcal{N}}(m_j) = n_i$.
 238 This led to a significant improvement in template matching.
 239

240 **Deformable Diversity Similarity** Building upon the
 241 above work, [26] added two additional and rather simple
 242 assumptions. The first of which is that the diversity of Near-
 243 est Neighbors between corresponding templates should be
 244 high. This is actually a prerequisite to a high best buddies
 245 similarity score and serves as a rough approximations. For
 246 this end diversity is formally defined as:
 247

$$DIS = c \cdot |\{n_i \in \mathcal{N} : \exists m_j \in \mathcal{M}, NN(m_j, \mathcal{N}) = n_i\}| \quad (1)$$

248 where $|\cdot|$ denotes group size and $c = 1/\min(|\mathcal{M}|, |\mathcal{N}|)$ is
 249 a normalization factor. Between non corresponding win-
 250 dows, indeed one should expect most points to have no real
 251 corresponding point, and thus be mapped to a very and re-
 252 mote nearest neighbors. On the other hand, regions contain-
 253 ing matching objects are drawn from the same distribution,
 254 thus the diversity of nearest neighbors should be high. To
 255 accommodate this assumption not only did they rewarded
 256 high diversity of nearest neighbors, but also penalized map-
 257 ping to the same patch. To this end, another, a negative
 258 diversity measure had been defined:
 259

$$\kappa(n_i) = |\{m \in \mathcal{M} : NN^a(m, \mathcal{N}) = n_i\}| \quad (2)$$

260 With x_i^a denoting the appearance descriptor of point x_i .
 261 Thus the contribution of being a nearest neighbor to a patch
 262 with multiple nearest neighbors would become $\exp(1 - \kappa(NN^a(m_j, \mathcal{N})))$. A final observation made has been that
 263 while non rigid deformations do occur, they should be re-
 264 stricted, small, in real objects. With the distance on the
 265 window pixel grid between 2 nearest neighbor points de-
 266 fined as $r_j = d(m_j^l, n_j^l)$ with x_i^l denoting the location of x_i
 267

268 relative to the center of the template, the final Deformable
 269 Diversity Similarity formulation becomes:
 270

$$DDIS = c \sum_{\mathcal{M} \leftarrow \mathcal{N}} \frac{1}{1 + r_j} \cdot \exp(1 - \kappa(NN^a(m_j, \mathcal{N}))) \quad (3)$$

271 3. Deformable Diversity for Partial matching 272 of 3D surfaces

273 **1. Goal of this section** In this section we will describe
 274 the Deformable Diversity framework for matching of de-
 275 formable shapes, as we had adjusted it for the 3D setting.
 276 The algorithm follows the ideas presented by [26], and ad-
 277 justs them for the unique challenges posed by the 3D setting
 278 in which information is sparser and of varying density, and
 279 the scenario of partial shape correspondence in which the
 280 part and the scene are of comparable area.
 281

282 **2. Key ideas of the algorithm** As stated above, a lot of
 283 the key ideas are similar to the 2D scenario - the feature
 284 nearest neighbor field between a part and his transformed
 285 version tends to give rise to a high diversity of matches. In
 286 addition, correct corresponding points between a template
 287 and a matching object should lie in nearby regions with
 288 relation to some reference point on the template. We im-
 289 prove upon these with the realization that while deforma-
 290 tion should hold very roughly for the entire part, it tends to
 291 hold better the closer we are to the reference point. This
 292 gives rise to a framework in which instead of matching the
 293 whole template at once, we break it into multiple tasks of
 294 smaller template matching, effectively using DDIS as a mid
 295 level psuedo-metric to describe part similarity. Finally we
 296 employ a strategy of choosing extremities on the surface for
 297 the central points of the mini templates. Picking these ex-
 298 tremities together with the matching of mini templates tends
 299 to both mitigate boundary effects, and pushes the size of the
 300 object in the full shape and the partial shape to be more sim-
 301 ilar. Finally, we observe that DDIS has different properties
 302 at different scales and thus employ a multi-scale cascade to
 303 take advantage of this fact.
 304

305 **3. Overview of the algorithm (Preprocessing (normal es-
 306 timation, FPFH), Finding the landmark points, computing
 307 DDIS correspondence for pairs, computing correspondence
 308 of surfaces) Include an image of this general overview.**
 309

310 The outline of the algorithm is as follows: we first cal-
 311 culate the nearest neighbor field between the full shape and
 312 the part - we begin by calculating local point descriptors
 313 and use ANN to find for each point $m_i \in \mathcal{M}$ its most similar
 314 point $NN^S(m_i, \mathcal{N})$. We then use an extremity locating al-
 315 gorithm to find suitable mini template centers. for each of
 316 those we extract a surface piece of a certain geodesic radius
 317 around it to serve as the mini template. Then for each of
 318 those templates we look for the most similar piece of surface
 319 of a similar radius around each point on \mathcal{M} . We use DDIS
 320 as a similarity measure between all pairs of mini templates.
 321

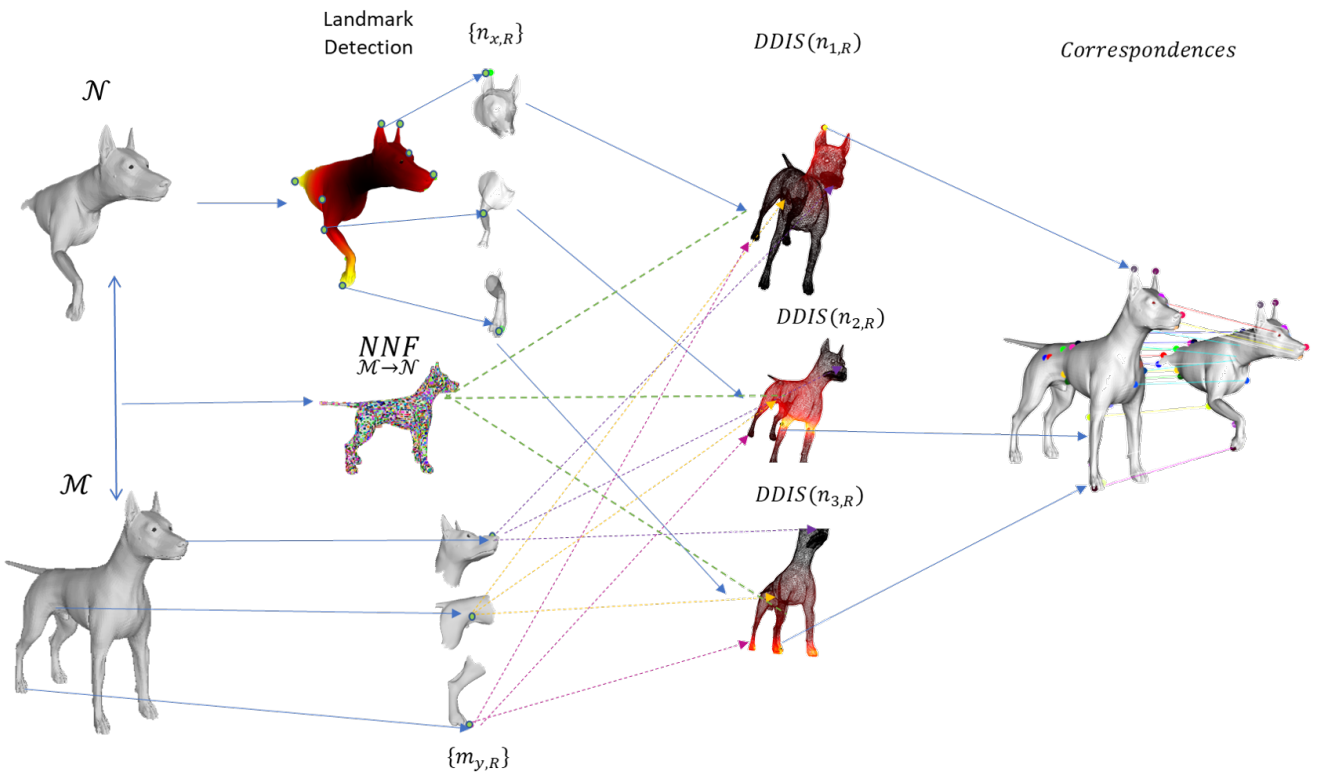


Figure 1. High level illustration of the DDIS Partial Correspondence pipe.

The points whose surface patch maximize this function for each mini template are then set as the corresponding points to their centers.

4. Road-map to the section We will begin with a description of the changes made for the deformable diversity framework as a result of moving from 2D to 3D. We will then go over the specific stages of preprocessing necessary for Deformable Diversity in 3D. We will continue with describing the matching process of a single mini template on a full shape. Finally we will describe the extraction of multiple correspondences using this framework.

3D Deformable Diversity Formulation

The nature of 3D data gives rise to unique problems which do not occur in the 2D scenario. Data is distributed in space both sparsely and with varying densities - the amount of data points occupying a given volume can vary drastically.

A second problem arises from the absence of a regular grid. These problems require different definitions for key components to the 2D deformable diversity formulation. For this work we chose the image patch to be replaced by a neighborhood which is required to calculate a selected shape descriptor, usually a small sphere in euclidean space or a surface patch in a small environment with a radius r_F . The search window of a template is replaced by a bigger environment around a chosen point, one which encompasses

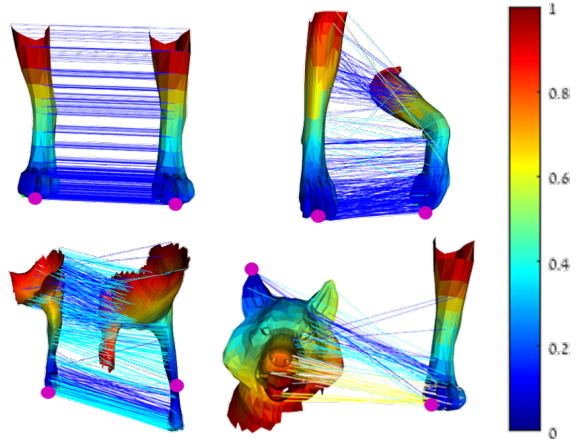


Figure 2. Illustration of Diversity Similarity between different shapes. Geodesic Distances are color coded by the jet scheme. You can notice that on identical pieces, and even on deformed matching pieces there are multiple diverse matches, most of which are colored in blue to indicate very similar distances from the source point, whereas on different pieces most lines map to very few points and a lot of yellow lines (high deformation) exist

the entire desired part ,with a radius denoted by R . The pixel grid distance is replaced by either a euclidean distance

432 $d_{Euc}(x^l, y^l)$ (in the case of point cloud) or geodesic distance
 433 $d_{Geo}(x^l, y^l)$ (for surface meshes). Given these DDIS
 434 between shape parts $\mathcal{M}_{x,R}$ and $\mathcal{N}_{y,R}$ can be naively formulated
 435 as:
 436

$$DDIS = c \cdot \sum_{m_j \in \mathcal{M}_{x,R}} \frac{\exp(1 - \kappa(NN^S(m_j, \mathcal{N}_{y,R}))}{1 + r_j} \quad (4)$$

440 where $\mathcal{M}_{x,R}$ and $\mathcal{N}_{y,R}$ are the shape parts in a radius R
 441 surrounding the points m_x and n_y respectively, and $r_j =$
 442 $|d(m_j^l, m_x^l) - d(NN^S(m_j, \mathcal{N}_{y,R})^l, n_y^l)| / (\gamma \cdot R)$, where γ
 443 is a tunable parameter and $c = 1/\min|\mathcal{N}_{y,R}|, |\mathcal{M}_{x,R}|$.
 444

445 However, we wouldn't like to penalize our similarity
 446 score in case of repeating patterns or symmetrical shapes
 447 which have both symmetries in the template search window.
 448 Intuitively and empirically the exponent is too harsh
 449 and indeed unnecessary as both deformity and diversity will
 450 attenuate the score in case of multiple nearest neighbors.
 451 On the other hand, we wouldn't want to reward far corre-
 452 spondences at all. **explain why – can we see it visually**
on the same example? no visual example yet, as the parti-
tion into smaller templates mitigates some of the problems
of the old formulation it seems, though the new one has
still given an extra 2 percent of accurate matches even in
the mini template setting To account for this the following
 453 formulation has been found to work better: given a point
 454 $n_i \subset \mathcal{N}_{y,R}$ has a set of points $\mathcal{M}_{n_i} = \{m_j \in \mathcal{M}_{j,R} : NN^S(m_j, \mathcal{N}_{y,R}) = n_i\}$ for which it is the nearest neighbor,
 455 we define $m'_i = \underset{m_j \in \mathcal{M}_{n_i}}{\operatorname{argmin}}(r_j)$ and r'_i the minimal dis-
 456 tortion distance our corrected formula becomes
 457

$$DDIS(\mathcal{N}_{y,R}, \mathcal{M}_{x,R}, \gamma) = \sum_{m'_i} \frac{1}{1 + r'_i} \quad (5)$$

464 This equation still promotes both diversity and low de-
 465 formations, but is less biased towards unsymmetrical surfaces.
 466

470 3.1. DDIS Template Matching

472 **Goal of the algorithm** In this section we go over the flow
 473 of template matching of 3D shapes using DDIS, the solution
 474 of which constitutes the core of our partial shape matching.
 475 Given a template $\mathcal{N}_{y,R}$ with a reference point n_y as its center
 476 and a maximal distance R , we aim to find on and object
 477 \mathcal{M} which has a deformed version of it, the corresponding
 478 surface piece $\mathcal{M}_{y*,R}$ and its center m_{y*} . The solution is
 479 obtained by finding the point on \mathcal{M} whose surrounding sur-
 480 face maximizes the above mentioned DDIS measure. **key**
 481 **ideas**

482 **Overview** We'll first give an overview, and then give an
 483 extended description of each of each stage.

484 We start by calculating the normals for \mathcal{M} and \mathcal{N} . We
 485 than calculate local patch descriptors for each patch of some

Algorithm 1 3DIS Correspondence

```

procedure DDIS MATCH( $\mathcal{M}, n_y, \mathcal{N}, R_{thresh}, NNF$ ) $\triangleright_{\mathcal{M} \rightarrow \mathcal{N}}$ 
  Returns the location of the  $n_i \subset \mathcal{N}$  in  $\mathcal{M}$ 
   $\mathcal{N}_{y,R} \leftarrow \{N_i \in \mathcal{N} : d_{Geo}(n_i, n_x) < R_{thresh}\}$ 
   $Similarity_{max} \leftarrow 0$ 
  for  $m_x \in \mathcal{M}$  do  $\triangleright$  DDIS calculation Loop
     $\mathcal{M}_{x,R} \leftarrow \{m_j \in \mathcal{M} : d_{Geo}(m_x, m_j) < 1.05 \cdot R_{thresh}\}$ 
     $Similarity[x] \leftarrow DDIS(\mathcal{M}_{x,R}, \mathcal{N}_{y,R})$ 
    if  $Similarity[x] > Similarity_{max}$  then
       $Similarity_{max} \leftarrow Similarity[x]$ 
       $m_y^* \leftarrow m_x$ 
    end if
  end for
  return  $m_y^*$ 
end procedure

```

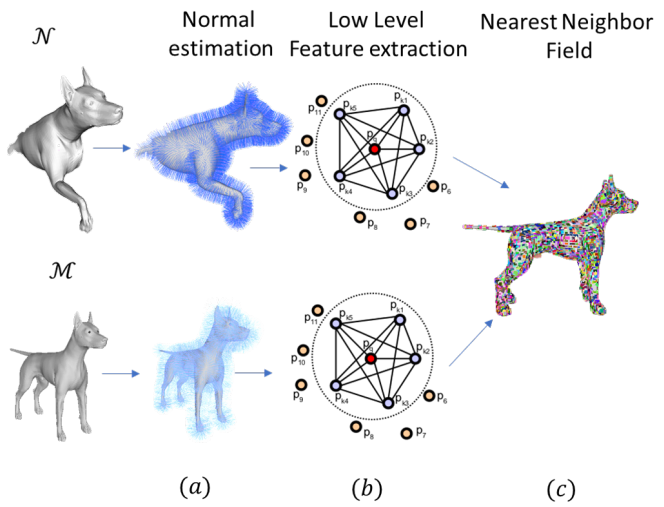


Figure 3. Nearest Neighbor Field calculation.

neighborhood around the points in each mesh (For our purpose FPFH seemed to work the best of our tested descriptors). Having calculated these descriptors we calculate a nearest neighbor field by finding for each patch in \mathcal{M} its Nearest Neighbor in \mathcal{N} . We now find the distance of every point $n \in \mathcal{N}$ to the desired point n_y for a desired neighborhood R . We now go over every point $m_x \in \mathcal{M}$. For each we extract the surface $\mathcal{M}_{x,R}$ in an R neighborhood around it. We take notice that while the above stages are done here in the context of template matching for one template, when matching multiple templates all of the above calculations have to be done only once between the shapes, with the exception of geodesic distance field extraction for the template itself.

Now we calculate our DDIS similarity measure of this surface with $\mathcal{N}_{x,R}$ which has n_y as its center. Having done

486
 487
 488
 489
 490
 491
 492
 493
 494
 495
 496
 497
 498
 499
 500
 501
 502
 503
 504
 505
 506
 507
 508
 509
 510
 511
 512
 513
 514
 515
 516
 517
 518
 519
 520
 521
 522
 523
 524
 525
 526
 527
 528
 529
 530
 531
 532
 533
 534
 535
 536
 537
 538
 539

540 that for every location, the point m_y* which gets the maximal DDIS Score is deemed the corresponding point to n_y
 541
 542
 543
 544
 545
 546
 547
 548
Point Normal Estimation There are various schemes
 for the estimation of point normals given a triangulated
 mesh surface. We have picked the one which is available in
 the standard PCL. Given a vertex p_i on a triangulated mesh
 \mathcal{X} and it's associated polygons $\{A_j\}_{j=1}^k$ and their normals
 N_{A_j} the point normal $N_i = \sum_{j=1}^k |A_j| \cdot N_{A_j}$

549 **Local Patch Size choice** DDIS as defined by [] uses
 550 patch descriptors as low level features for their similarity
 551 measure. While a patch in an image can be defined by
 552 the images grid no such grid exists on 3D point clouds and
 553 meshes, where density of data points can vary. Thus a patch
 554 has to be defined by some geometric measure. While the
 555 more robust way to define it would be using geodesic dis-
 556 tance, since we are talking a small environment around a
 557 point on the mesh we have found that for practical purposes
 558 a patch in a defined euclidean radius around a point serves
 559 well enough. We pick this radius in the following way:
 560 given the full surface mesh \mathcal{M} we define a characteristic
 561 length $D_{\mathcal{M}} = \sqrt{\text{Area}(\mathcal{M})}$, and tune a parameter α to ob-
 562 tain $r_F = \frac{\alpha}{100} * D_{\mathcal{M}}$

563 **Local Patch Descriptor** A lot of local shape descrip-
 564 tors have been used successfully in 3D shape analysis.
 565 We have tested the following descriptors which are in-
 566 cluded in the Point Cloud Library: ROPS[?, Theorem
 567 2] PFH[] SHOT[], HKS[], SIHKS[], ROPS[] and FPFH[].
 568 Out of these 4 FPFH has achieved the best performance,
 569 and thus the descriptor for the local patch has been cho-
 570 sen to be FPFH. **Nearest Neighbor Field** As an inter-
 571 mediate stage towards the calculation of Deformable Di-
 572 versity Similarity measure, the calculation of the near-
 573 est neighbor field(will be abbreviated as NNF) needs to
 574 be calculated. Thus for every patch $m \in \mathcal{M}$ we have
 575 to find the patch on the template $n \in \mathcal{N}$ which resem-
 576 bles it the most. For $FPFH, NNS(m_j, \mathcal{N})$ is defined
 577 $NNS(m_j, \mathcal{N}) \equiv \underset{i}{\operatorname{argmin}} \chi^2(FPFH(m_j), FPFH(n_i))$
 578 and the Nearest Neighbor Field is the set of all these cor-
 579 respondences.

580 **DDIS calculation** For every point in $m_x \in \mathcal{M}$ we then
 581 extract a surface part $\mathcal{M}_{x,R}$ with a radius R around it and
 582 calculate deformable diversity around it. The point which
 583 maximizes DDIS gives us a correspondence (n_y, m_y*) .
 584 Since as we will show in the results section, imperfections
 585 in the isometry assumption lead to considerable localiza-
 586 tion errors, we move to a multiple template matching framework
 587 using DDIS, as will be described in the next section.

588 3.2. DDIS Sparse Correspondences

589 A key takeaway from experimenting with DDIS as a
 590 template matching algorithm for partial matching has been
 591 that isometry does not hold, at least not globally. It does

592 however, hold pretty well locally, especially at extremities.
 593 To this end we devise multiple template framework for Par-
 594 tial correspondences of deformable shape. We first obtain
 595 the landmarks $F = \{f\}_i$ as described in []. We then choose
 596 a partiality radius $R = \gamma \cdot R$ and extract surface parts $\mathcal{N}_{i,R}$
 597 around each extremity point. Finally for each point we cal-
 598 culate DDIS to get it's correspondence.

599 **Landmark Extraction** We follow the work of [Sagi
 600 Katz Ayallet Tal] to obtain interesting landmark points.
 601 Given a shape the work employs the following framework
 602 to extract it's extremities. A point is detected as an extre-
 603 mity if it fulfills 2 conditions: - it's sum of geodesic distances
 604 is a local extrema, formally, for $v \in S$, where S is a surface
 605 mesh, we define the set of points with a direct edge to it as
 606 N_v , the point is a critical point if :

$$\sum_{v_i \in S} d_{geo}(v, v_i) > \sum_{v_i \in S} d_{geo}(v_n, v_i), \forall v_n \in N_v \quad (6)$$

607 An additional requirement for it to be an extremities is for
 608 it to lie on the convex hull of the shape's MDS. In this work
 609 we have dropped the last condition, but chose N_v* - a neigh-
 610 borhood of $0.03 \cdot \sqrt{\text{Area}(S)}$.

611 Algorithm 2 3DIS Sparse Correspondences

```
612 procedure DDIS CORRESPONDENCE( $\mathcal{M}, \mathcal{N}, \alpha, \beta, \gamma$ )  

  613   Returns point correspondence for critical points on  $\mathcal{N}$   

  614    $r_F \leftarrow \alpha / 100 \cdot \sqrt{\text{Area}(\mathcal{M})}$   

  615    $R_{thresh} \leftarrow \beta / 100 \cdot \sqrt{\text{Area}(\mathcal{M})}$   

  616    $N_{\mathcal{M}} \leftarrow \text{ComputeNormals}(\mathcal{M})$   

  617    $N_{\mathcal{N}} \leftarrow \text{ComputeNormals}(\mathcal{N})$   

  618    $F_{\mathcal{M}} \leftarrow FPFH(\mathcal{M}, N_{\mathcal{M}}, r_F)$   

  619    $F_{\mathcal{N}} \leftarrow FPFH(\mathcal{N}, N_{\mathcal{N}}, r_F)$   

  620    $NNF_{\mathcal{M} \rightarrow \mathcal{N}} \leftarrow ANN(F_{\mathcal{M}}, F_{\mathcal{N}})$   

  621    $\mathcal{N}_c = \{n : \sum_{n_i \in \mathcal{N}} d_{geo}(n, n_i) > \sum_{n_i \in \mathcal{N}} d_{geo}(n, n_i), \forall n \in \mathcal{N}\}$   

  622    $n_{y*} \leftarrow DDIS\_Correspondence(\mathcal{M}, n_y, \mathcal{N}, \alpha, \beta, \gamma)$   

  623   for  $n_y \in \mathcal{N}_c$  do ▷ DDIS calculation Loop  

  624      $m_{c*} \leftarrow DDIS\_Correspondence(\mathcal{M}, n_y, \mathcal{N}, \alpha, \beta, \gamma)$   

  625   end for  

  626   return  $\mathcal{M}_c \times \mathcal{N}_c = \{m_{c*}, n_c\}$   

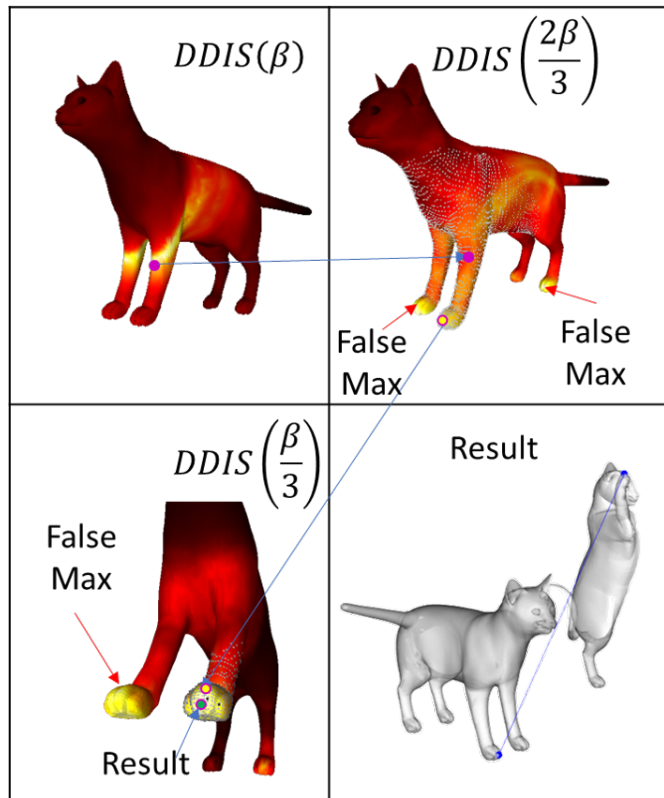
  627 end procedure
```

628 **Landmark Template Matching** For this end, we create
 629 a template for each landmark point - we collect all surface
 630 point in a geodesic neighborhood around it of $\beta \cdot \sqrt{\text{area}(\mathcal{M})}$
 631 where for this case a good β (0.2, 0.5) where larger beta
 632 prevents global scale error, such as a cats paw being mapped
 633 to a hind paw, while smaller beta promotes tighter localiza-
 634 tion on the part itself. This can be seen in Figure[] While it
 635 might seem natural to calculate a different nearest neighbor
 636 field for each landmark template it has been empirically
 637 found that using the global nearest neighbor field gives

648 much better results. This is probably due to the fact that the
 649 nearest neighbor field encodes global information when ob-
 650 tained this way and eliminates local distractors. Each land-
 651 mark template is compared to all surface parts of a similar
 652 R on \mathcal{M} to obtain final point correspondences.
 653

654 3.3. Cascaded Multi-Scale DDIS

655 The observation of the effects of the choice of β and the
 656 trade-off between finer localization and avoidance of global
 657 errors naturally leads to the adoption of a multi scale frame-
 658 work. We calculate *DDIS* score for multiple *beta* values,
 659 and use the location obtained with a large beta to select a
 660 narrow environment in which we look for the maximum
 661 of DDIS with a smaller value *beta*, thus using the larger
 662 scale to get a rough global location, and the smaller scale
 663 to fit it into a more exact location. While this might be
 664 done at multiple custom scales we have found that the triplet
 665 $\beta, 2 \cdot \beta/3, \beta/3$ works well.
 666



693 Figure 4. Illustration of the multi scale framework. Gray point are
 694 the area chosen by the previous scale to be valid. It can be seen
 695 that Wrong maxima in lower scales are ignored due to this process
 696

697 4. Experiments and results

698 In this section we will briefly go over the experiments
 699 performed and their results. We'll introduce the datasets,
 700

702 detail our experiments and their results
 703

704 4.1. Datasets

705 In this section we will briefly go over the available
 706 Datasets
 707

708 4.1.1 SHREC 2016

709 The SHREC partial matching dataset consists of 8 base,
 710 neutral pose models: cat, centaur, dog, horse, wolf, and
 711 3 humans 2 males, and 1 female. Each basic model has
 712 corresponding deformed partial shapes obtained either by
 713 cutting the shape with a plane or by adding holes on a de-
 714 formed shape. The set has been divided into train and test
 715 sets. The train set is composed of 15 cuts for each base
 716 models totaling 120 models, and 10 holed shpaes for each
 717 model for which ground truth point to polygon correspon-
 718 dences has been provided in barycentric coordinates. The
 719 test set is composed of additional 200 cuts and 200 holed
 720 shapes.
 721

722 4.2. Error Metrics

723 The output of partial matching algorithms (as defined
 724 in[8]) are sub-vertex point-to-point correspondences be-
 725 tween partial shapes. For all experiments we use the stan-
 726 dard practice of not penalizing symmetric solutions. Qual-
 727 ity is measured according to the Princeton benchmark pro-
 728 tocol [11]. For a pair of points $(x, y) \in \mathcal{N} \times \mathcal{M}$ between
 729 the full object \mathcal{M} and the partial shape \mathcal{N} produced by an
 730 algorithm, where (x, y^*) is the ground truth correspondence
 731 the inaccuracy is measured by
 732

$$\varepsilon(x) = \frac{d_{\mathcal{M}}(y, y^*)}{\sqrt{\text{area}(\mathcal{M})}} \quad (7)$$

733 where $d_{\mathcal{M}}(y, y^*)$ is the geodesic distance on \mathcal{M} , and has
 734 units of normalized length on \mathcal{M} . For dense correspon-
 735 dences over a dataset, $\varepsilon(x)$ is averaged over all matching
 736 instances.
 737

738 4.2.1 Central Points Localization

739 In this experiment we have chosen for each Template mesh
 740 the center point c_T and tried to match it to a point on the ob-
 741 ject using DDIS. Experiments have been done using FPFH,
 742 PFH and SHOT as patch descriptors with patch radiiuses of
 743 [2, 3, 4, 5], the results of the opimal parameter for each de-
 744 scriptor are illustrated in fig. and visualizations of simila-
 745 rity maps of cuts are provided in fig. . It can be seen that
 746 good localization is obtained for points on a smooth sur-
 747 face, under high partiality conditions and strong deforma-
 748 tions. Bad matches occur when a matched point resides on
 749 a heavily deformed patch, and when salient anchor points
 750 are deformed or cut. Analysis of these results shows a drift
 751

756

757

758

759

760

761

762

763

764

765

766

767

768

769

770

771

772

773

774

775

776

777

778

779

780

781

782

783

784

785

786

787

788

789

790

791

792

793

794

795

796

797

798

799

800

801

802

803

804

805

806

807

808

809

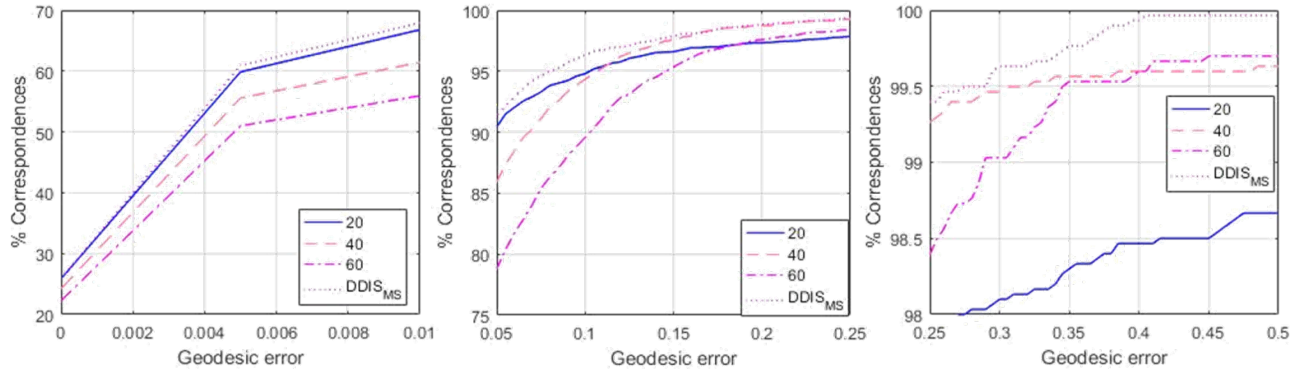


Figure 5. Effect of the β parameter on the results: it can be seen that a smaller beta promotes better localization in a small neighborhood, while higher values of β lead to more local errors but are more robust to global errors. It can be seen that the multi-scale cascade achieves better results both locally and globally.

in localization occurs when salient features are divided by strong unisometric deformations which serve as the motivation for the multiple template matching framework.

4.3. Sparse Correspondences on the SHREC16 Test set

In this experiment we have tested the performance of DDIS in producing sparse correspondences on the SHREC16 Partial Matching of Deformable Shapes competition. We had tuned our parameters on the SHREC16 training dataset using only the cuts part of it. The best results had been produced using FPFH with $r_F = 0.04\sqrt{\text{Area}(\mathcal{M})}$, and a piece size radius $R_{thresh} = 0.3\sqrt{\text{Area}(\mathcal{M})}$. For Geodesic distances we have found the fast marching algorithm to work the fastest, while giving the lowest error w.r.t. to exact geodesics. For a 10,000 vertices mesh it takes 60s to produce a full distance matrix, Though it should be noted this algorithm has a more efficient GPU implementation. FPFH and Nearest Neighbor field takes 2 s' and similarity between 2 pieces of 10000 vertices each takes 25s on average, running on a single thread of i7-2700k. Unlike optimization based algorithms this is highly parallelizable. We achieve results comparable to the state of the art [13] quality wise, even though sparser in nature on both the Cuts and the Holes datasets, Where a particularly impressive result is reported on the Holes dataset. A further look reveals even more reliable results can be obtained taking only the extremity points not lying on the mesh longest boundary, but they will be more sparse

	PFM	RF	IM	EN	GT	DIS	DISnoBound
cuts	dense	dense	61.3	87.8	51.0	27.9	14.5
holes	dense	dense	78.2	112.6	76.4	77.3	52.11

Table 1. mean number of correspondence obtained by the algorithms in the SHREC 16 competiton and our algorithm

References

- [1] D. Aiger, N. J. Mitra, and D. Cohen-Or. 4pointss congruent sets for robust pairwise surface registration. *ACM Trans. Graph.*, 27(3):85:1–85:10, Aug. 2008. 2
- [2] N. Aigerman, R. Poranne, and Y. Lipman. Seamless surface mappings. *ACM Transactions on Graphics (TOG)*, 34(4):72, 2015. 2
- [3] M. Aubry, U. Schlickewei, and D. Cremers. The wave kernel signature: A quantum mechanical approach to shape analysis. In *Computer Vision Workshops (ICCV Workshops), 2011 IEEE International Conference on*, pages 1626–1633. IEEE, 2011. 2
- [4] A. M. Bronstein and M. M. Bronstein. Not only size matters: regularized partial matching of nonrigid shapes. In *Computer Vision and Pattern Recognition Workshops, 2008. CVPRW’08. IEEE Computer Society Conference on*, pages 1–6. IEEE, 2008. 1, 2
- [5] A. M. Bronstein, M. M. Bronstein, A. M. Bruckstein, and R. Kimmel. Partial similarity of objects, or how to compare a centaur to a horse. *International Journal of Computer Vision*, 84(2):163, 2009. 2
- [6] A. M. Bronstein, M. M. Bronstein, and R. Kimmel. Generalized multidimensional scaling: a framework for isometry-invariant partial surface matching. *Proceedings of the National Academy of Sciences*, 103(5):1168–1172, 2006. 1, 2
- [7] M. M. Bronstein and I. Kokkinos. Scale-invariant heat kernel signatures for non-rigid shape recognition. In *Computer Vision and Pattern Recognition (CVPR), 2010 IEEE Conference on*, pages 1704–1711. IEEE, 2010. 2
- [8] L. Cosmo, E. Rodolà, M. Bronstein, A. Torsello, D. Cremers, and Y. Sahillioglu. Shrec16: Partial matching of deformable shapes. *Proc. 3DOR*, 2, 2016. 1, 7
- [9] T. Dekel, S. Oron, M. Rubinstein, S. Avidan, and W. T. Freeman. Best-buddies similarity for robust template matching. In *Proceedings of the IEEE Conference on Computer Vision and Pattern Recognition*, pages 2021–2029, 2015. 3
- [10] D. Holz, A. E. Ichim, F. Tombari, R. B. Rusu, and S. Behnke. Registration with the point cloud library: A modular frame-

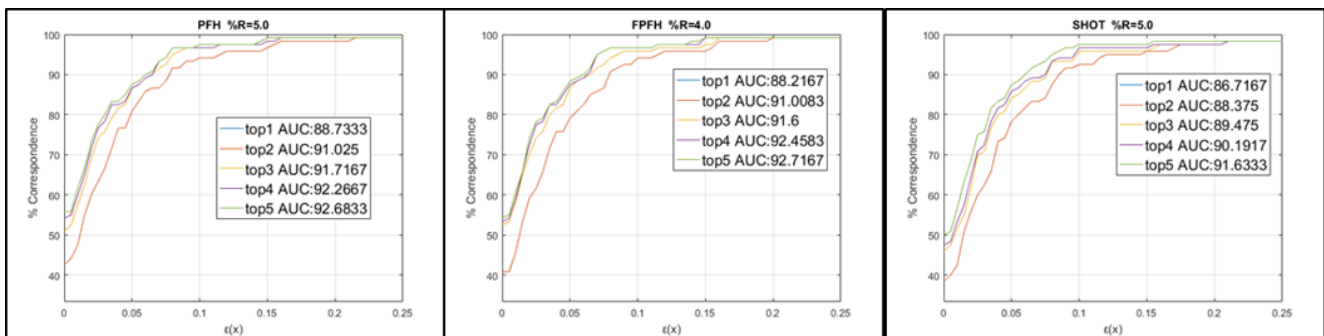
864
865
866
867
868
869
870
871
872
873
874

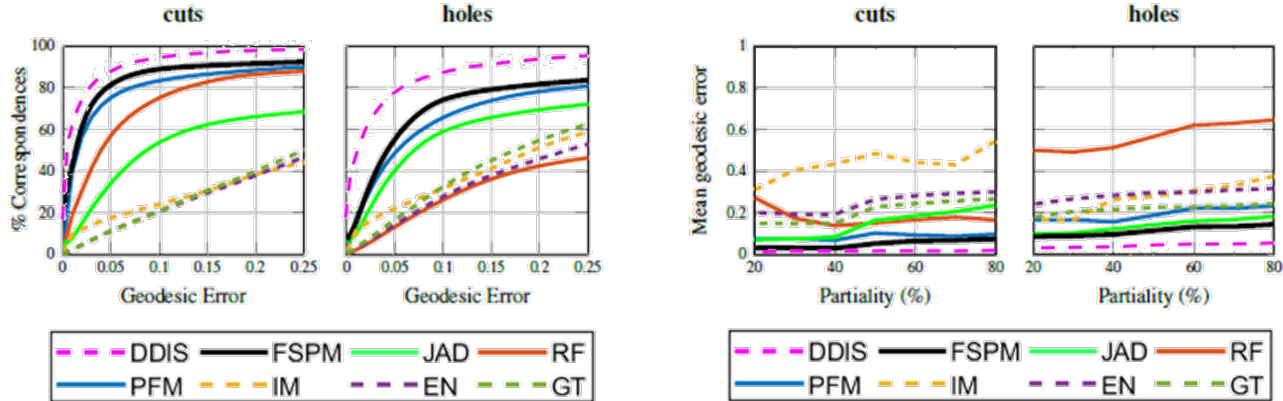
Figure 6. Comparison between descriptors: we show curves for the minimal distance of the top results. a noticeable addition occurs when adding the 2nd best match

877

878
879

With Boundary Points

880



881

882

883

884

885

886

887

888

889

890

891

892

893

894

895

896

897

898

899

900

901

902

903

904

905

906

907

908

909

910

911

912

913

914

915

916

917

918

919

920

921

922

923

924

925

926

927

928

929

930

931

932

933

934

935

936

937

938

939

940

941

942

943

944

945

946

947

948

949

950

951

952

953

954

955

956

957

958

959

960

961

962

963

964

965

966

967

968

969

970

971

894

895

896

897

898

899

900

901

902

903

904

905

906

907

908

909

910

911

912

913

914

915

916

917

Discarding Boundary Points

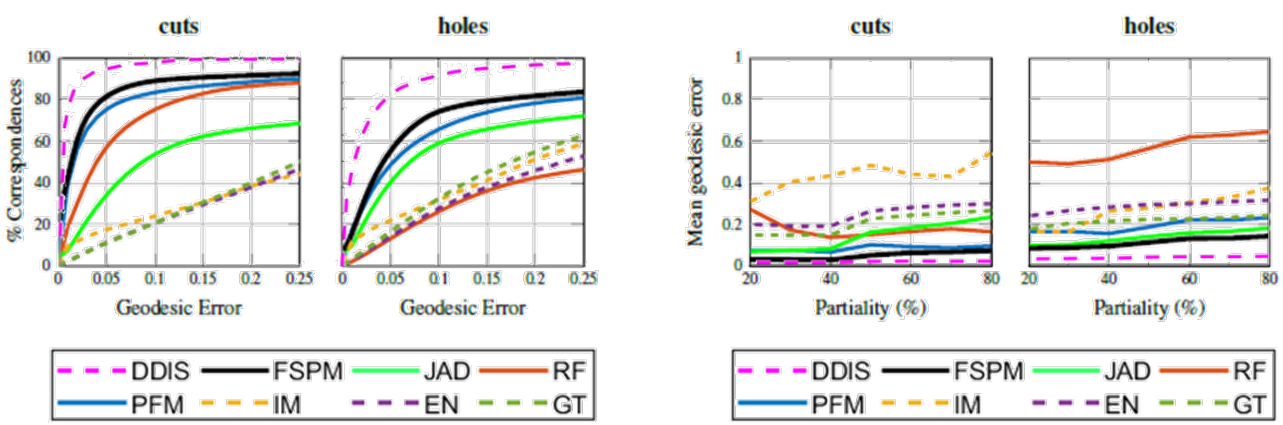


Figure 7. comparison with other state of the art algorithms - it can be seen that although sparse in nature, the correspondence obtained by DDIS are much more accurate than the other methods. A separate analysis has been done for correspondences which include boundary points, which tend to be more noisy, and internal points which are more sparse

work for aligning in 3-d. *IEEE Robotics & Automation Magazine*, 22(4):110–124, 2015. 1

[11] V. G. Kim, Y. Lipman, and T. Funkhouser. Blended intrinsic maps. In *ACM Transactions on Graphics (TOG)*, volume 30,

page 79. ACM, 2011. 7

- [12] A. Kovnatsky, M. M. Bronstein, X. Bresson, and P. Vandergheynst. Functional correspondence by matrix completion. In *Proceedings of the IEEE conference on computer*

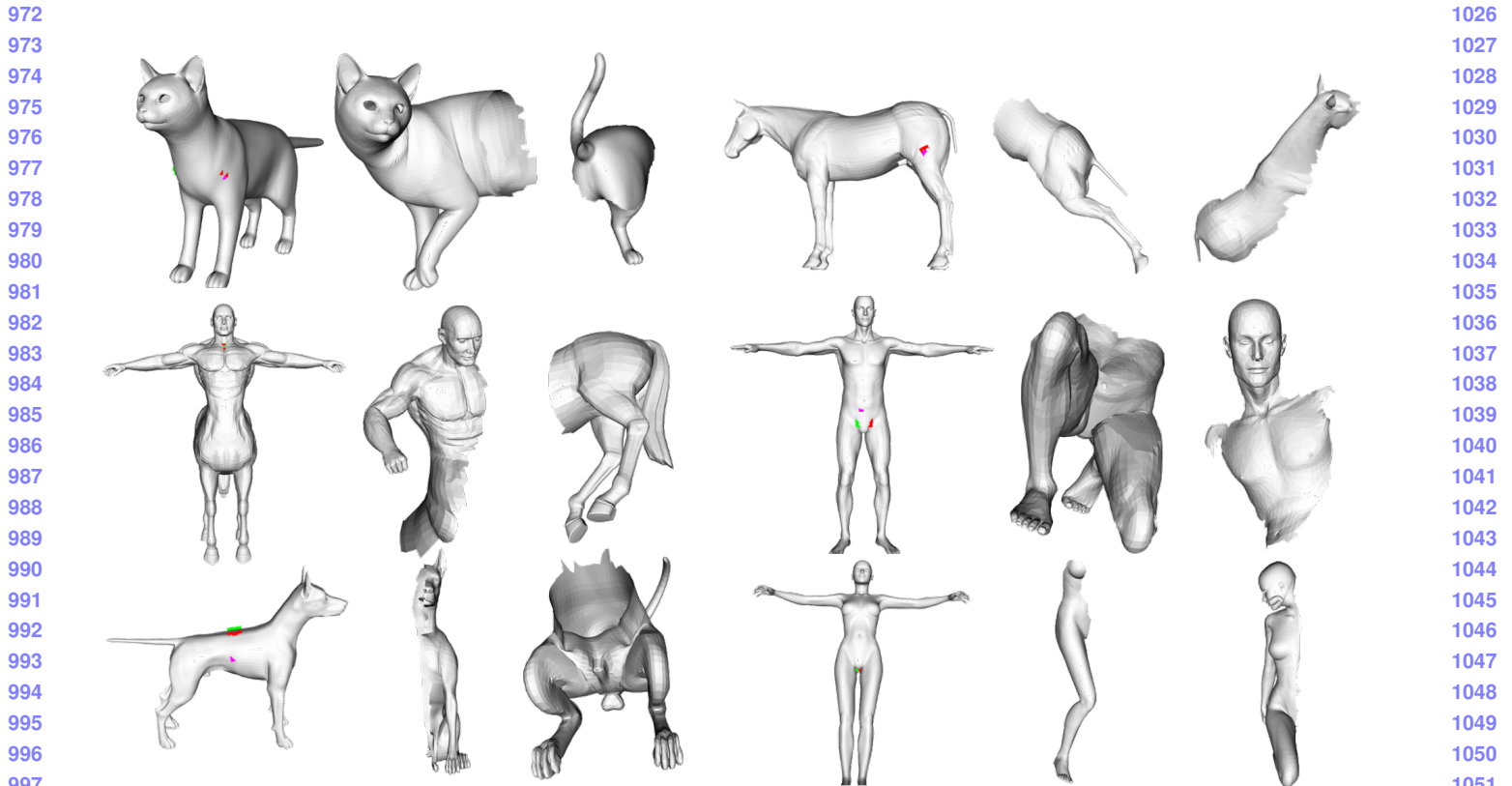


Figure 8. SHREC 16 cuts partial matching dataset.

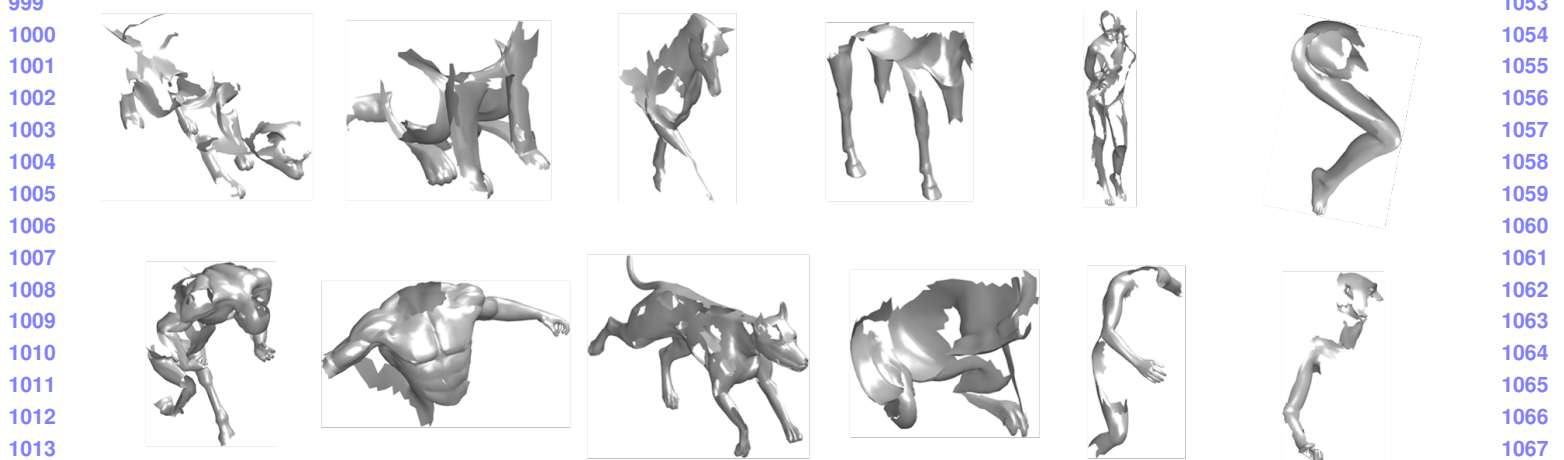


Figure 9. SHREC 16 holes partial matching dataset.

vision and pattern recognition, pages 905–914, 2015. 2

- 1018 [13] O. Litany, E. Rodolà, A. M. Bronstein, and M. M. Bronstein.
1019 Fully spectral partial shape matching. In *Computer Graphics
1020 Forum*, volume 36, pages 247–258. Wiley Online Library,
1021 2017. 1, 2, 8
- 1022 [14] H. Maron, N. Dym, I. Kezurer, S. Kovalsky, and Y. Lip-
1023 man. Point registration via efficient convex relaxation. *ACM
1024 Transactions on Graphics (TOG)*, 35(4):73, 2016. 2
- 1025 [15] M. Ovsjanikov, M. Ben-Chen, J. Solomon, A. Butscher, and

L. Guibas. Functional maps: A flexible representation of
maps between shapes. *ACM Trans. Graph.*, 31(4):30:1–
30:11, July 2012. 1, 2

- [16] J. Pokrass, A. M. Bronstein, and M. M. Bronstein. Partial
shape matching without point-wise correspondence. *Nu-
merical Mathematics: Theory, Methods and Applications*,
6(1):223–244, 2013. 2
- [17] J. Pokrass, A. M. Bronstein, M. M. Bronstein, P. Sprech-
mann, and G. Sapiro. Sparse modeling of intrinsic cor-

- 1080 respondences. In *Computer Graphics Forum*, volume 32,
1081 pages 459–468. Wiley Online Library, 2013. 2
 1082 [18] E. Rodolà, L. Cosmo, M. M. Bronstein, A. Torsello, and
1083 D. Cremers. Partial functional correspondence. In *Computer
1084 Graphics Forum*, volume 36, pages 222–236. Wiley Online
1085 Library, 2017. 1, 2
 1086 [19] E. Rodolà, A. Torsello, T. Harada, Y. Kuniiyoshi, and D. Cre-
1087 mers. Elastic net constraints for shape matching. In *Pro-
1088 ceedings of the IEEE International Conference on Computer
1089 Vision*, pages 1169–1176, 2013. 2
 1090 [20] R. B. Rusu, N. Blodow, and M. Beetz. Fast point feature
1091 histograms (fpfh) for 3d registration. In *Robotics and Au-
1092 tomation, 2009. ICRA'09. IEEE International Conference
1093 on*, pages 3212–3217. Citeseer, 2009. 1, 2
 1094 [21] R. B. Rusu, Z. C. Marton, N. Blodow, and M. Beetz. Learn-
1095 ing informative point classes for the acquisition of object
1096 model maps. In *Control, Automation, Robotics and Vi-
1097 sion, 2008. ICARCV 2008. 10th International Conference
1098 on*, pages 643–650. IEEE, 2008. 2
 1099 [22] R. B. Rusu, Z. C. Marton, N. Blodow, M. Dolha, and
1100 M. Beetz. Towards 3d point cloud based object maps for
1101 household environments. *Robotics and Autonomous Sys-
1102 tems*, 56(11):927–941, 2008. 2
 1103 [23] Y. Sahillioglu and Y. Yemez. Scale normalization for iso-
1104 metric shape matching. In *Computer Graphics Forum*, vol-
1105 ume 31, pages 2233–2240. Wiley Online Library, 2012. 2
 1106 [24] Y. Sahillioglu and Y. Yemez. Multiple shape correspond-
1107 ence by dynamic programming. In *Computer Graphics Forum*,
1108 volume 33, pages 121–130. Wiley Online Library, 2014. 2
 1109 [25] J. Solomon, G. Peyré, V. G. Kim, and S. Sra. Entropic metric
1110 alignment for correspondence problems. *ACM Transac-
1111 tions on Graphics (TOG)*, 35(4):72, 2016. 2
 1112 [26] I. Talmi, R. Mechrez, and L. Zelnik-Manor. Template match-
1113 ing with deformable diversity similarity. In *Proc. of IEEE
1114 Conf. on Computer Vision and Pattern Recognition*, pages
1311–1319, 2017. 1, 3
 1115 [27] A. Torsello. A game-theoretic approach to deformable shape
1116 matching. In *Proceedings of the 2012 IEEE Conference on
1117 Computer Vision and Pattern Recognition (CVPR), CVPR
1118 '12*, pages 182–189, Washington, DC, USA, 2012. IEEE
1119 Computer Society. 1, 2
 1120 [28] M. Vestner, Z. Lähner, A. Boyarski, O. Litany, R. Slossberg,
1121 T. Remez, E. Rodolà, A. Bronstein, M. Bronstein, R. Kimmel,
1122 et al. Efficient deformable shape correspondence via
1123 kernel matching. In *3D Vision (3DV), 2017 International
1124 Conference on*, pages 517–526. IEEE, 2017. 1, 2
 1125 [29] M. Vestner, R. Litman, E. Rodolà, A. M. Bronstein, and
1126 D. Cremers. Product manifold filter: Non-rigid shape corre-
1127 spondence via kernel density estimation in the product space.
1128 In *CVPR*, pages 6681–6690, 2017. 2
- 1129 **References**
- 1130 [1] D. Aiger, N. J. Mitra, and D. Cohen-Or. 4pointss congruent
1131 sets for robust pairwise surface registration. *ACM Trans.
1132 Graph.*, 27(3):85:1–85:10, Aug. 2008. 2
- 1133 [2] N. Aigerman, R. Poranne, and Y. Lipman. Seamless surface
1134 mappings. *ACM Transactions on Graphics (TOG)*, 34(4):72,
1135 2015. 2
- 1136 [3] M. Aubry, U. Schlickewei, and D. Cremers. The wave kernel
1137 signature: A quantum mechanical approach to shape analy-
1138 sis. In *Computer Vision Workshops (ICCV Workshops), 2011
1139 IEEE International Conference on*, pages 1626–1633. IEEE,
1140 2011. 2
- 1141 [4] A. M. Bronstein and M. M. Bronstein. Not only size mat-
1142 ters: regularized partial matching of nonrigid shapes. In
1143 *Computer Vision and Pattern Recognition Workshops, 2008.
1144 CVPRW'08. IEEE Computer Society Conference on*, pages
1145 1–6. IEEE, 2008. 1, 2
- 1146 [5] A. M. Bronstein, M. M. Bronstein, A. M. Bruckstein, and
1147 R. Kimmel. Partial similarity of objects, or how to compare a
1148 centaur to a horse. *International Journal of Computer Vision*,
1149 84(2):163, 2009. 2
- 1150 [6] A. M. Bronstein, M. M. Bronstein, and R. Kimmel. Gener-
1151 alized multidimensional scaling: a framework for isometry-
1152 invariant partial surface matching. *Proceedings of the Na-
1153 tional Academy of Sciences*, 103(5):1168–1172, 2006. 1, 2
- 1154 [7] M. M. Bronstein and I. Kokkinos. Scale-invariant heat ker-
1155 nel signatures for non-rigid shape recognition. In *Computer
1156 Vision and Pattern Recognition (CVPR), 2010 IEEE Confer-
1157 ence on*, pages 1704–1711. IEEE, 2010. 2
- 1158 [8] L. Cosmo, E. Rodolà, M. Bronstein, A. Torsello, D. Cremers,
1159 and Y. Sahillioglu. Shrec16: Partial matching of deformable
1160 shapes. *Proc. 3DOR*, 2, 2016. 1, 7
- 1161 [9] T. Dekel, S. Oron, M. Rubinstein, S. Avidan, and W. T. Free-
1162 man. Best-buddies similarity for robust template matching.
1163 In *Proceedings of the IEEE Conference on Computer Vision
1164 and Pattern Recognition*, pages 2021–2029, 2015. 3
- 1165 [10] D. Holz, A. E. Ichim, F. Tombari, R. B. Rusu, and S. Behnke.
1166 Registration with the point cloud library: A modular frame-
1167 work for aligning in 3-d. *IEEE Robotics & Automation Maga-
1168 zine*, 22(4):110–124, 2015. 1
- 1169 [11] V. G. Kim, Y. Lipman, and T. Funkhouser. Blended intrinsic
1170 maps. In *ACM Transactions on Graphics (TOG)*, volume 30,
1171 page 79. ACM, 2011. 7
- 1172 [12] A. Kovnatsky, M. M. Bronstein, X. Bresson, and P. Van-
1173 derghenst. Functional correspondence by matrix comple-
1174 tion. In *Proceedings of the IEEE conference on computer
1175 vision and pattern recognition*, pages 905–914, 2015. 2
- 1176 [13] O. Litany, E. Rodolà, A. M. Bronstein, and M. M. Bronstein.
1177 Fully spectral partial shape matching. In *Computer Graphics
1178 Forum*, volume 36, pages 247–258. Wiley Online Library,
1179 2017. 1, 2, 8
- 1180 [14] H. Maron, N. Dym, I. Kezurer, S. Kovalsky, and Y. Lip-
1181 man. Point registration via efficient convex relaxation. *ACM
1182 Transactions on Graphics (TOG)*, 35(4):73, 2016. 2
- 1183 [15] M. Ovsjanikov, M. Ben-Chen, J. Solomon, A. Butscher, and
1184 L. Guibas. Functional maps: A flexible representation of
1185 maps between shapes. *ACM Trans. Graph.*, 31(4):30:1–
1186 30:11, July 2012. 1, 2
- 1187 [16] J. Pokrass, A. M. Bronstein, and M. M. Bronstein. Partial
1188 shape matching without point-wise correspondence. *Nu-
1189 merical Mathematics: Theory, Methods and Applications*,
1190 6(1):223–244, 2013. 2

- 1188 [17] J. Pokrass, A. M. Bronstein, M. M. Bronstein, P. Sprechmann, and G. Sapiro. Sparse modeling of intrinsic correspondences. In *Computer Graphics Forum*, volume 32, pages 459–468. Wiley Online Library, 2013. 2 1242
1189 1243
1190 1244
1191 1245
1192 [18] E. Rodolà, L. Cosmo, M. M. Bronstein, A. Torsello, and D. Cremers. Partial functional correspondence. In *Computer Graphics Forum*, volume 36, pages 222–236. Wiley Online Library, 2017. 1, 2 1246
1193 1247
1194 1248
1195 1249
1196 [19] E. Rodola, A. Torsello, T. Harada, Y. Kuniyoshi, and D. Cremers. Elastic net constraints for shape matching. In *Proceedings of the IEEE International Conference on Computer Vision*, pages 1169–1176, 2013. 2 1250
1197 1251
1198 1252
1199 1253
1200 [20] R. B. Rusu, N. Blodow, and M. Beetz. Fast point feature histograms (fpfh) for 3d registration. In *Robotics and Automation, 2009. ICRA'09. IEEE International Conference on*, pages 3212–3217. Citeseer, 2009. 1, 2 1254
1201 1255
1202 1256
1203 1257
1204 [21] R. B. Rusu, Z. C. Marton, N. Blodow, and M. Beetz. Learning informative point classes for the acquisition of object model maps. In *Control, Automation, Robotics and Vision, 2008. ICARCV 2008. 10th International Conference on*, pages 643–650. IEEE, 2008. 2 1258
1205 1259
1206 1260
1207 1261
1208 [22] R. B. Rusu, Z. C. Marton, N. Blodow, M. Dolha, and M. Beetz. Towards 3d point cloud based object maps for household environments. *Robotics and Autonomous Systems*, 56(11):927–941, 2008. 2 1262
1209 1263
1210 1264
1211 1265
1212 [23] Y. Sahillioğlu and Y. Yemez. Scale normalization for isometric shape matching. In *Computer Graphics Forum*, volume 31, pages 2233–2240. Wiley Online Library, 2012. 2 1266
1213 1267
1214 1268
1215 [24] Y. Sahillioğlu and Y. Yemez. Multiple shape correspondence by dynamic programming. In *Computer Graphics Forum*, volume 33, pages 121–130. Wiley Online Library, 2014. 2 1269
1216 1270
1217 1271
1218 [25] J. Solomon, G. Peyré, V. G. Kim, and S. Sra. Entropic metric alignment for correspondence problems. *ACM Transactions on Graphics (TOG)*, 35(4):72, 2016. 2 1272
1219 1273
1220 [26] I. Talmi, R. Mechrez, and L. Zelnik-Manor. Template matching with deformable diversity similarity. In *Proc. of IEEE Conf. on Computer Vision and Pattern Recognition*, pages 1311–1319, 2017. 1, 3 1274
1221 1275
1222 1276
1223 1277
1224 [27] A. Torsello. A game-theoretic approach to deformable shape matching. In *Proceedings of the 2012 IEEE Conference on Computer Vision and Pattern Recognition (CVPR)*, CVPR '12, pages 182–189, Washington, DC, USA, 2012. IEEE Computer Society. 1, 2 1278
1225 1279
1226 1280
1227 1281
1228 1282
1229 [28] M. Vestner, Z. Lähner, A. Boyarski, O. Litany, R. Slossberg, T. Remez, E. Rodola, A. Bronstein, M. Bronstein, R. Kimmel, et al. Efficient deformable shape correspondence via kernel matching. In *3D Vision (3DV), 2017 International Conference on*, pages 517–526. IEEE, 2017. 1, 2 1283
1230 1284
1231 1285
1232 1286
1233 [29] M. Vestner, R. Litman, E. Rodolà, A. M. Bronstein, and D. Cremers. Product manifold filter: Non-rigid shape correspondence via kernel density estimation in the product space. In *CVPR*, pages 6681–6690, 2017. 2 1287
1234 1288
1235 1289
1236 1290
1237 1291
1238 1292
1239 1293
1240 1294
1241 1295

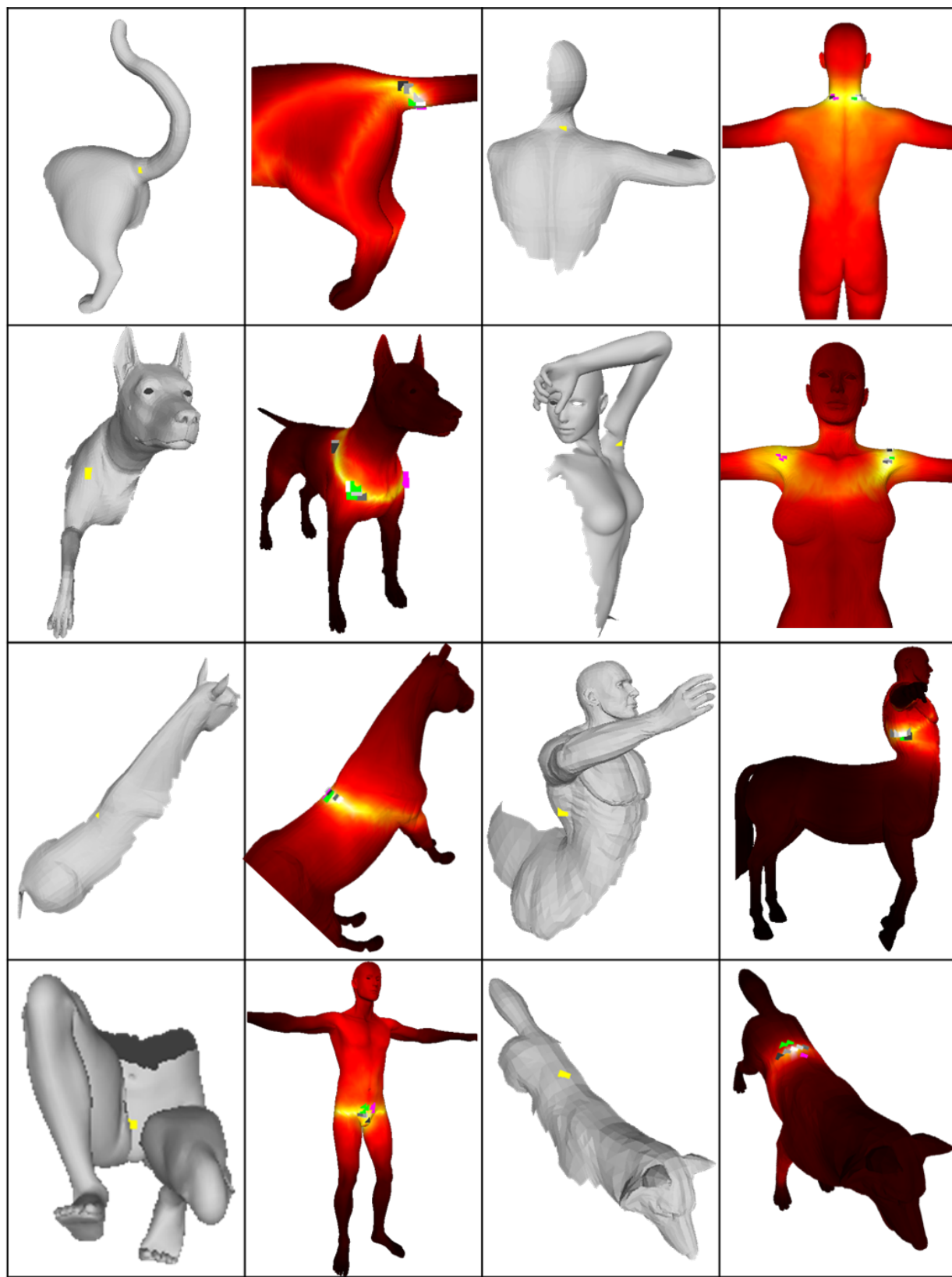
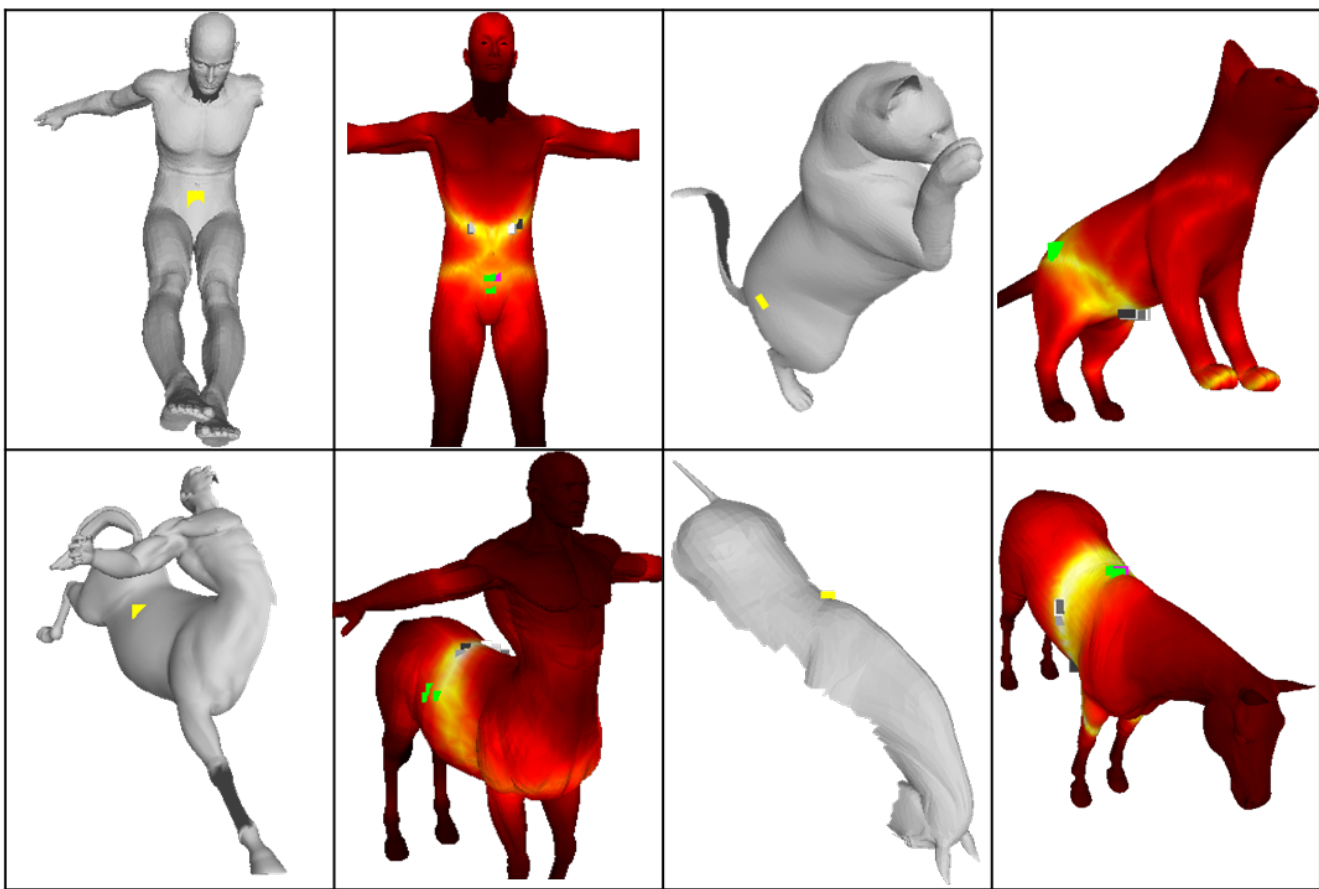
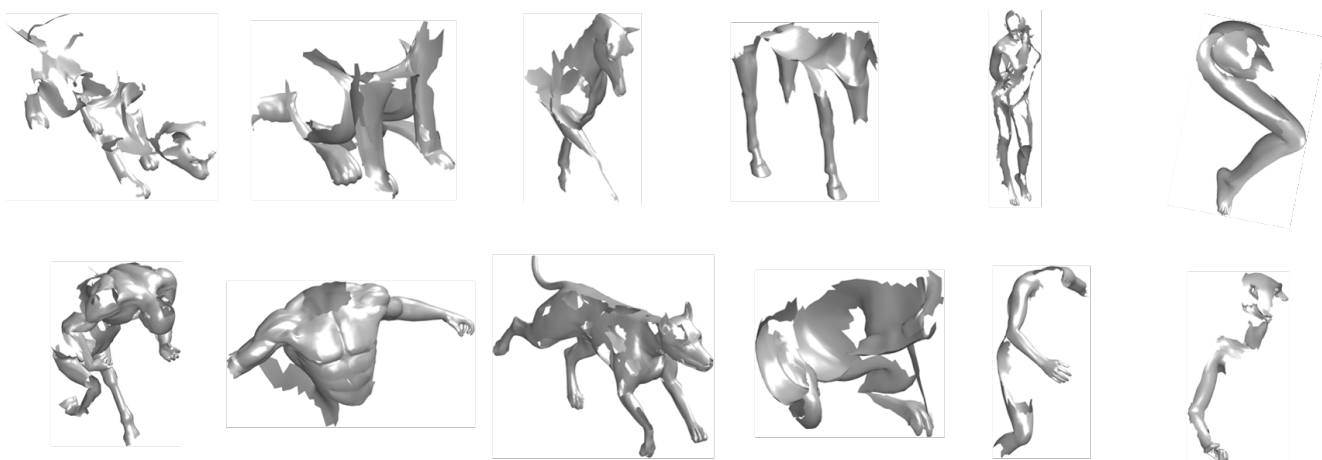


Figure 10. Some examples of cuts and their matching similarity score maps. The compared point is marked in yellow on the cut, whereas ground truth polygon is marked in green, symmetrical polygon in purple, and top 5 matches in grayscale

1296
1297
1298
1299
1300
1301
1302
1303
1304
1305
1306
1307
1308
1309
1310
1311
1312
1313
1314
1315
1316
1317
1318
1319
1320
1321
1322
1323
1324
1325
1326
1327
1328
1329
1330
1331
1332
1333
1334
1335
1336
1337
1338
1339
1340
1341
1342
1343
1344
1345
1346
1347
1348
1349
1350
1351
1352
1353
1354
1355
1356
1357
1358
1359
1360
1361
1362
1363
1364
1365
1366
1367
1368
1369
1370
1371
1372
1373
1374
1375
1376
1377
1378
1379
1380
1381
1382
1383
1384
1385
1386
1387
1388
1389
1390
1391
1392
1393
1394
1395
1396
1397
1398
1399
1400
1401
1402
1403

1404
1405
1406
1407
1408
1409
1410
1411
1412
1413
1414
1415
1416
1417
1418
1419
14201421
1422
1423
1424
1425
1426
1427
1428
1429
1430
1431
1432
1433
1434
1435
1436
1437
1438
1439
1440
1441
1442
1443
1444
1445
1446
1447
1448
1449
1450
1451
1452
1453
1454
1455
1456
1457
1458
1459
1460
1461
1462
1463
1464
1465
1466
1467
1468
1469
1470
1471
1472
1473
1474
1475
1476
1477
1478
1479
1480
1481
1482
1483
1484
1485
1486
1487
1488
1489
1490
1491
1492
1493
1494
1495
1496
1497
1498
1499
1500
1501
1502
1503
1504
1505
1506
1507
1508
1509
1510
15111458
1459
1460
1461
1462
1463
1464
1465
1466
1467
1468
1469
1470
1471
1472
1473
1474
1475
1476
1477
1478
1479
1480
1481
1482
1483
1484
1485
1486
1487
1488
1489
1490
1491
1492
1493
1494
1495
1496
1497
1498
1499
1500
1501
1502
1503
1504
1505
1506
1507
1508
1509
1510
1511

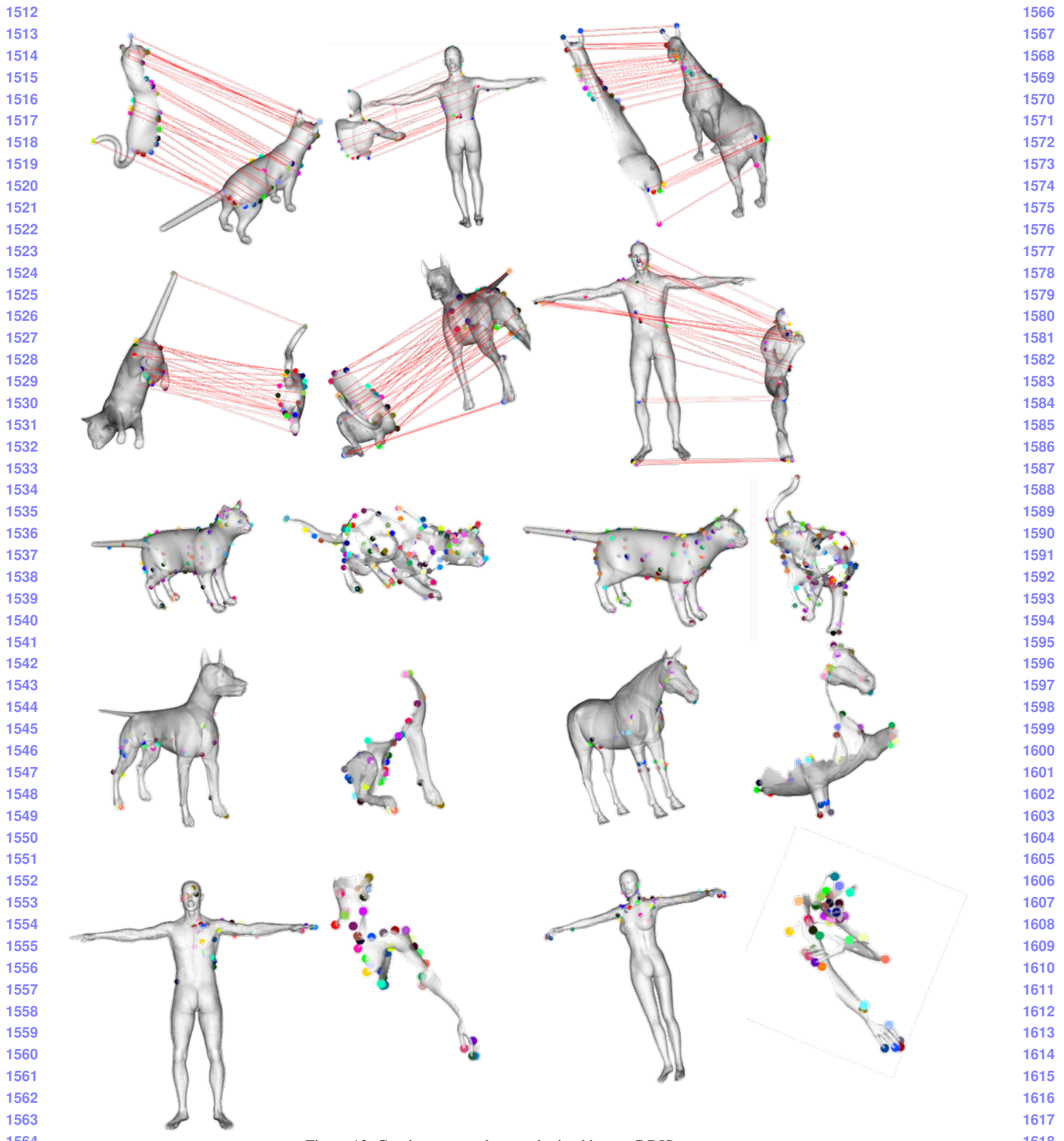


Figure 13. Good correspondences obtained by our DDIS measure

1620
1621
1622
1623
1624
1625
1626
1627
1628
1629
1630
1631
1632
1633
1634
1635
1636
1637
1638
1639
1640
1641
1642
1643
1644
1645
1646
1647
1648
1649
1650
1651
1652
1653
1654
1655
1656
1657
1658
1659
1660
1661
1662
1663
1664
1665
1666
1667
1668
1669
1670
1671
1672
1673

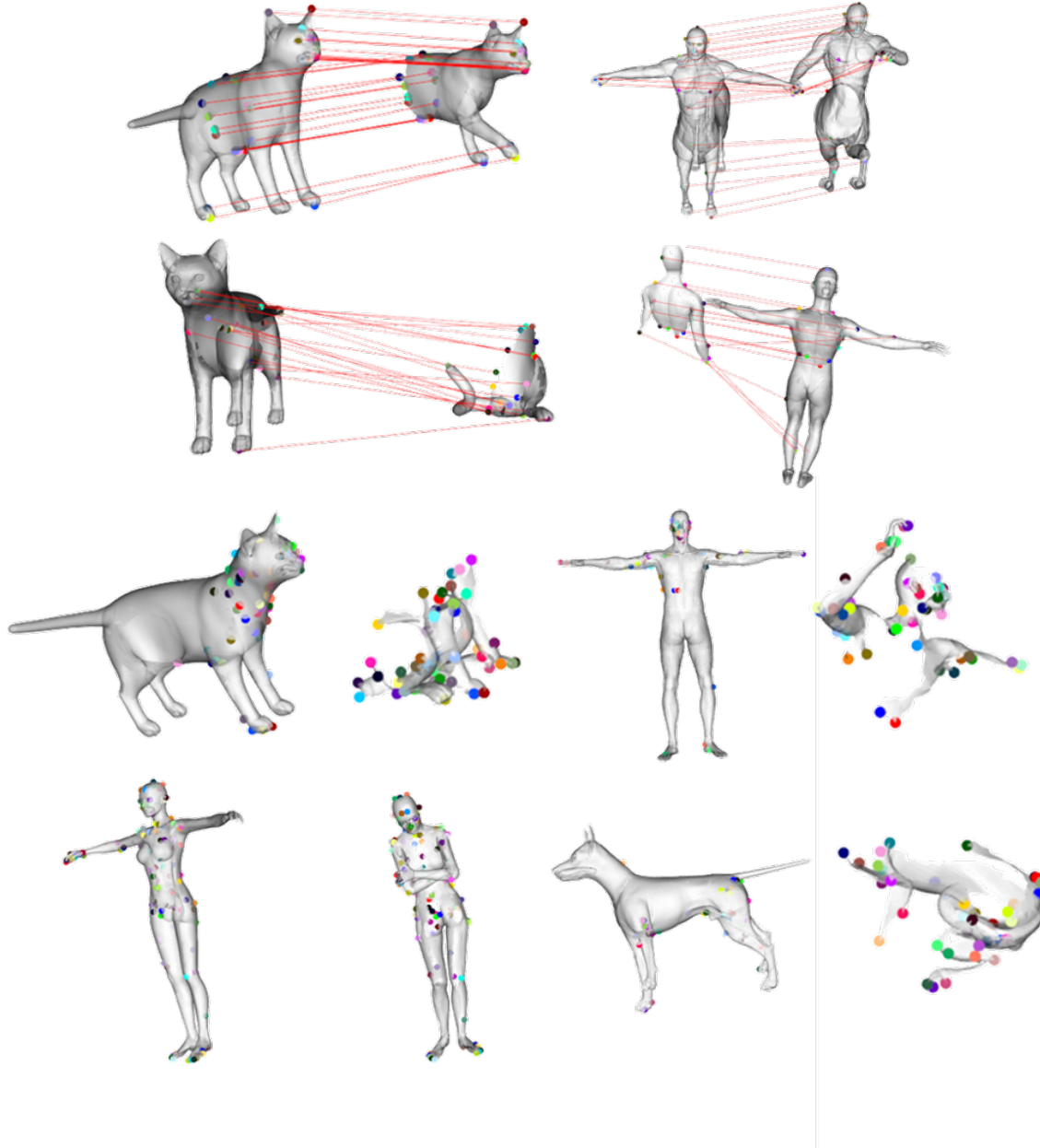


Figure 14. Some notable failure cases - most common is cat paw assignment - an extrinsic near symmetry gives rise to this phenomena. Closed fists on humanoids tends to cause a collapse of all fingers to a single finger. In the holes extreme partiality makes the geodesic distances break even over short distances.

1674
1675
1676
1677
1678
1679
1680
1681
1682
1683
1684
1685
1686
1687
1688
1689
1690
1691
1692
1693
1694
1695
1696
1697
1698
1699
1700
1701
1702
1703
1704
1705
1706
1707
1708
1709
1710
1711
1712
1713
1714
1715
1716
1717
1718
1719
1720
1721
1722
1723
1724
1725
1726
1727